American Mineralogist, Volume 58, pages 444–450, 1973

The Polarized Spectra of Iron in Silicates. I. Enstatite

W. Alan Runciman, Dipankar Sengupta, and Marc Marshall

Department of Solid State Physics, Research School of Physical Sciences, The Australian National University, Canberra, A.C.T., 2600, Australia

Abstract

Polarization spectra covering infrared, visible and ultraviolet ranges from 2200-27000 cm^{-1} have been obtained of enstatite at room and liquid helium temperatures. The main features of these spectra are described in terms of a set of assignments of crystal field levels and a theory of intensities which involves the mixing of a charge transfer state into the $3d^6$ states of the ferrous ion. This better accounts for the features of the polarized absorption spectra of ferrous ion in pyroxenes than do the explanations of Bancroft and Burns (1967) and White and Keester (1967).

Introduction

There have been three previous attempts to explain the polarized spectra of ferrous iron in pyroxenes. White and Keester (1966) attributed the main absorption at 10800 cm^{-1} to ferrous iron in octahedral surroundings, but ascribed the band at 5400 cm^{-1} to ferrous iron in tetrahedral surroundings. Bancroft and Burns (1967) assigned both bands to octahedrally coordinated ions, the longer wavelength band being assigned to a transition within the ground octahedral $^5T_2$ configuration. White and Keester (1967) pointed out an error in the group theoretical classification of Bancroft and Burns, but were unable to provide a fully acceptable alternative. This is not surprising as they also used an incorrect classification of states. The present proposal assigns both bands to transitions from the ground state to the upper ^5E states of ferrous iron in octahedral coordination, as does Burns (1970). The crystal structure and polarized spectra for enstatite will be described in the next sections. The treatment with slight modification is applicable to many other silicates, and olivine will be considered in Part II (Runciman, Sengupta, and Gourley, 1973).

Absorption Spectra of Enstatite

A green gemstone of enstatite, probably from Kimberley, South Africa, was cut into a block of about $1.7\times1.1\times4.0$ mm oriented along the α, β and γ axes. Electron microprobe analysis indicates that the sample may be described as a solid solution containing 92.6 mole percent enstatite, 6.7 mole percent orthoferrosilite and 0.7 mole percent wollastonite. The complete analysis in weight percent is:

SiO_2,	57.68;	FeO,	4.63;	CaO,	0.36;
TiO_2,	<0.05;	MnO,	<0.05;	Na_2O,	0.51;
Al_2O_3,	0.82;	MgO,	35.84;	Cr_2O_3,	0.22.

Polarized spectra were obtained through the long faces α-γ and β-γ. Spectra for the three polarization directions were normalized to a thickness of 1 mm and are presented in Figure 1 for the crystal at room temperature. The range 2200–4000 cm^{-1} was covered using a Perkin-Elmer Model 180 infrared spectrophotometer. A liquid helium cryostat with CsI windows was fitted into the sample compartment for the low temperature runs. A Cary Model 17 spectrophotometer was used for the range 4000–27000 cm^{-1}, a flow-tube with a fused silica section being inserted into the sample compartment for measurements at liquid helium temperature. Polarized spectra were obtained using Glan-Taylor prisms. All the spectra have been redrawn using a wave-number scale. Intense absorption due to lattice vibrations prevents measurements below 2200 cm^{-1}. The results are in broad agreement with the unpolarized spectra of White and Keester (1966) and the polarized spectra of Bancroft and Burns (1967). The polarization properties of the infrared bands in the 2200–4000 cm^{-1} range have not been reported previously. The narrow bands from 3500 to 3650 cm^{-1} may be due to traces of OH in the crystal. The relative intensity of the β peak at 5400 cm^{-1} to the β peak at 10800 cm^{-1} is almost 2, whereas Burns (1970) shows the ratio about 1.2. The α peak at 10800 cm^{-1} is shown by Burns (1970, Fig. 5.6) to have a single maximum; but due to difficulty in thinning the

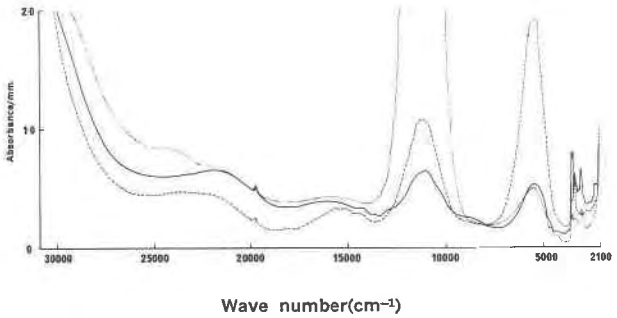

FIG. 1. Room temperature spectrum of enstatite ···· α spectrum, - - - β spectrum, —— γ spectrum.

crystal, which has good cleavage in {210} planes, this spectrum was not obtained in the present investigation. There are no major changes as the temperature is lowered to liquid helium temperature, but some of the peaks are better resolved. Regions with fine structure are shown in more detail with the crystal cooled in Figures 2 and 3. The narrow band at 506 nm is used for identification purposes by gemmologists. At liquid helium temperature it is located at 19780±10 cm^{-1} with a half-width of 40 cm^{-1}.

Crystal Structure

Enstatite, $(Mg,Fe)SiO_3$, has an orthorhombic crystal structure *Pcba* (no. 61) with 16 formula units per cell, $a_o = 8.829$Å, $b_o = 18.22$Å, $c_o = 5.192$Å. The crystal and optic axes are related by $\alpha = b, \beta = a, \gamma = c$. All atoms are in $(8c)$ positions, which have C_1 point symmetry. Ghose (1965) studied an intermediate orthopyroxene, $Mg_{0.93}Fe_{1.07}Si_2O_6$, and found that the $M(1)$ site had 15 percent Fe^{2+} and the $M(2)$ site had 90 percent Fe^{2+}. Both sites have octahedral coordination, but the $M(2)$ site shows greater distortion. This occurs since two of the oxygen atoms are bonded to two silicon atoms, whereas the other four are bonded to one silicon atom each. The interatomic distances are shown in Figure 4, labelling of the oxygen atoms being consistent with Ghose (1965), and the existence of a pseudo-twofold axis noted following earlier papers. The approximate point group is C_{2v}. The X,Y,Z axes used in discussion of the crystal field are shown, and the relationship to the α, β, γ axes will be described later.

Crystal Field Analysis

The major distortion of the $M(2)$ site is the elongation of two metal-oxygen bonds $M(2)$-O(3) and $M(2)$-O(6). Hence the approximate reduced symmetry is C_{2v}. It is often helpful to consider the symmetry chain from the full octahedral symmetry. In this case it is:

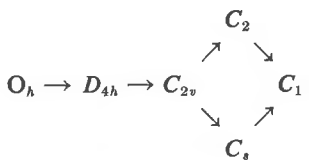

The pseudo-fourfold axis is the Y axis which is parallel to the shortest metal-oxygen bonds $M(2)$-O(5) and $M(2)$-O(2). This axis has been used for quantization when considering the possible effects of

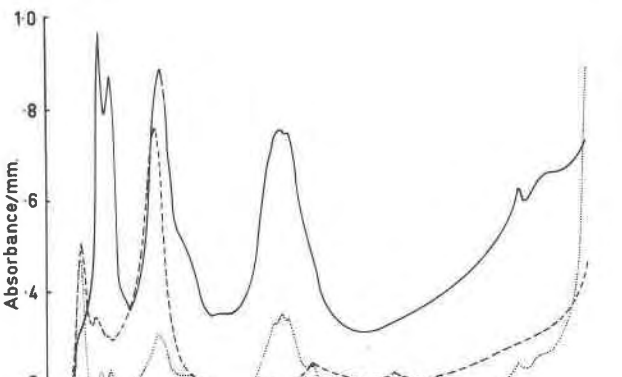

FIG. 2. 2200-3700 cm^{-1} helium temperature spectrum of enstatite ···· α spectrum, - - - β spectrum, —— γ spectrum.

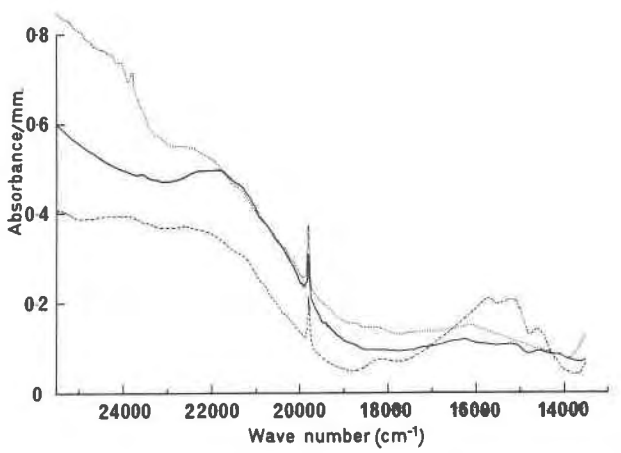

FIG. 3. 14000-25000 cm^{-1} helium temperature spectrum of enstatite ···· α spectrum, - - - β spectrum, —— γ spectrum.

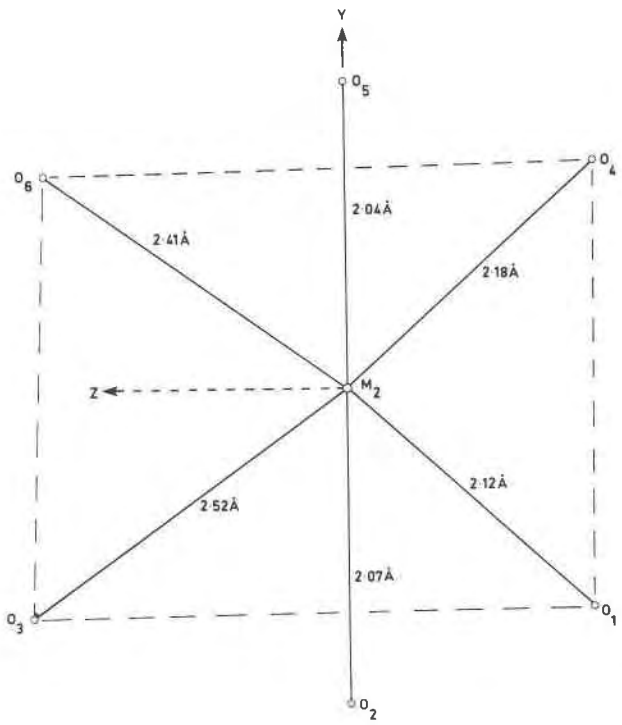

FIG. 4. $M(2)$ site and coordinate system.

spin-orbit interaction, but for simple crystal field calculations the Z axis is chosen as the major axis as it is the axis of highest symmetry.

The confusion in the literature has arisen at the stage of reducing the symmetry from $D_{4h} \rightarrow C_{2v}$. Depending on the distortion of the octahedron, there are four possibilities; the correlations for the even states are listed in Table 1, extracted from the larger table in Wilson, Decius, and Cross (1955). Column 4 is applicable to the distortion present in enstatite. Previously Bancroft and Burns (1967) used the correlation shown in column 2, which they obtained from Cotton (1963), whereas White and Keester (1967) used column 3. The selection rules for electric dipole transitions in C_{2v} symmetry are shown in

TABLE 1. Correlation Table for $D_{4h} \rightarrow C_{2v}$

D_{4h}	(1) C_2, σ_v	(2) C_2, σ_d	(3) C_2'	(4) C_2''
A_{1g}	A_1	A_1	A_1	A_1
A_{2g}	A_2	A_2	B_1	B_1
B_{1g}	A_1	A_2	A_1	B_1
B_{2g}	A_2	A_1	B_1	A_1
E_g	B_1+B_2	B_1+B_2	A_2+B_2	A_2+B_2

TABLE 2. Selection Rules for Electric Dipole Transitions in C_{2v} Symmetry

	A_1	A_2	B_1	B_2
A_1	Z	.	X	Y
A_2	.	Z	Y	X
B_1	X	Y	Z	.
B_2	Y	X	.	Z

Table 2, and using these the energy level diagram of Figure 5 is constructed. The $A_1 \rightarrow A_2$ transition, which is forbidden in C_{2v} symmetry, is shown dotted, as it will be allowed in C_1 symmetry.

Expressions for these levels in terms of a crystal field model have been calculated using the Z axis of Figure 4 as the axis of quantization. Only even crystal field terms need be considered so the symmetry of the crystal field potential is D_{2h}. It seems reasonable to consider the field as a distorted octahedral field. A perturbation approach suggests that the second order terms may be the most significant. Fourth order perturbation terms had to be neglected; otherwise two extra parameters are needed and the number of parameters becomes excessive. The crys-

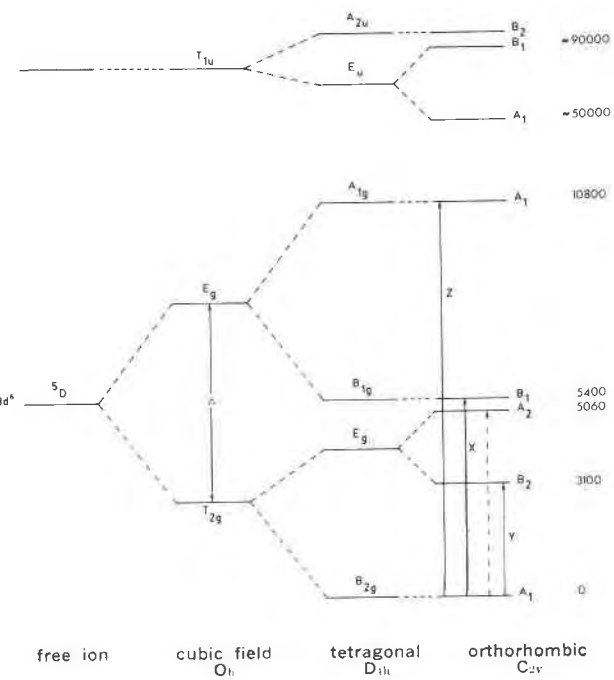

FIG. 5. Energy level scheme.

tal field potential then consists of the cubic field term Δ and second order term given by

$$B_2^0 C_2^0 + B_2^2 (C_2^2 + C_2^{-2})$$

where

$$C_k^q = \left[\frac{4\pi}{2k+1}\right]^{1/2} Y_k^q.$$

The expressions are simplified if auxiliary parameters δ_1 and δ_2 are introduced where

$$\delta_1 = \frac{B_2^0}{7} \quad \text{and} \quad \delta_2 = \frac{\sqrt{6}B_2^2}{7}.$$

The A_1 energy levels are given by the eigenvalues of the following matrix

$$\begin{bmatrix} 0.6\,\Delta - \delta_1 - \delta_2 & -\sqrt{3}\,\delta_1 + \delta_2/\sqrt{3} \\ -\sqrt{3}\,\delta_1 + \delta_2/\sqrt{3} & -0.4\,\Delta + \delta_1 + \delta_2 \end{bmatrix}.$$

The expressions for the energies of the states are listed in Table 3. Since there are two A_1 states, these will contain mixtures of the octahedral basis functions shown, which are expressed in terms of x, y, and z coordinate axes which are the axes of the coordination octahedron. The pseudo-fourfold short axis is z and corresponds to Y.

By fitting the allowed transitions, the following parameters in units of cm^{-1} are deduced:

$$\Delta = 5280, \qquad \delta_1 = -1150, \qquad \delta_2 = -1490.$$

These lead to the energy levels shown in Figure 5. This scheme differs considerably from previous schemes including that in Burns (1970). There is no clear sign of a band due to the transition to the A_2 level at 5060 cm^{-1}. This band is expected to be weak and could be hidden under the broad 5400 cm^{-1} band, since the transition is forbidden in C_{2v} symmetry.

Polarization Properties

The relationship between X, Y, Z and α, β, γ axes needs to be established to calculate the polarization ratios. The twofold axis (Z) is taken to be along the bisector of the angle O(6)-M(2)-O(3). According to Ghose (1965) the Z-axis then lies in or close to the α-γ plane and makes an angle of 22° with α axis. The β direction is close to a threefold axis of the coordination $M(2)$ octahedron.

TABLE 3. Crystal Field Splitting of ^{5}D Levels

O_h	C_{2v}	Wave Function	Energy
Eθ	A_1	$\frac{1}{2}(2z^2 - x^2 - y^2)$	$0.1\Delta + [0.25\Delta^2 - (\delta_1 + \delta_2)\Delta + (\delta_1 + \delta_2)^2 + (\sqrt{3}\delta_1 - \delta_2/\sqrt{3})^2]^{\frac{1}{2}}$
Eϵ	B_1	$\frac{\sqrt{3}}{2}(x^2 - y^2)$	$0.6\Delta + \delta_1 + \delta_2$
T_{2X}	A_2	$\sqrt{\frac{3}{2}}(zx - yz)$	$-0.4\Delta - 2\delta_1$
T_{2Z}	B_2	$\sqrt{\frac{3}{2}}(yz + zx)$	$-0.4\Delta + \delta_1 - \delta_2$
T_{2Y}	A_1	$\sqrt{3}\,xy$	$0.1\Delta - [0.25\Delta^2 - (\delta_1 + \delta_2)\Delta + (\delta_1 + \delta_2)^2 + (\sqrt{3}\delta_1 - \delta_2/\sqrt{3})^2]^{\frac{1}{2}}$

The Eulerian angles relating to the two coordinate systems are $\theta = 68°$, $\phi = 55°$ and $\psi = 0°$. The polarization intensities are proportional to the squares of the direction cosines. The calculated intensities corresponding to the above axes are given under columns marked Set 1 in Table 4. The 10800 cm^{-1} band is Z-polarized and hence should be strongly β with some γ and α, whereas the 3100 cm^{-1} band is Y-polarized and should be strongly γ with some β and α. The main peaks in all cases are correctly explained, but the relative intensities of subsidiary peaks do not match with experimental results. The best possible fit to the experimental intensities was obtained by treating the Eulerian angles as variable. The final values of the angles are $\theta = 70°$, $\phi = 63°$, $\psi = 35°$. The corresponding intensity values are shown under Set 2 in Table 4.

Spin-Orbit Splitting

In the above discussion we have neglected the effects of spin-orbit interaction. A detailed calcula-

TABLE 4. Experimental and Theoretical Polarization Intensities

Band	3100 cm^{-1} (Y)			5400 cm^{-1} (X)			10800 cm^{-1} (Z)		
Polarization	Experimental	Theoretical Set 1	Set 2	Experimental	Theoretical Set 1	Set 2	Experimental†	Theoretical Set 1	Set 2
α	0.29	0.10	0.26	0.15	0.05	0.15	0.69	0.85	0.59
β	0.19	0.33	0.04	0.68	0.67	0.67	0.19	0.02	0.30
γ	0.52	0.58	0.70	0.17	0.29	0.18	0.12	0.14	0.12

†The bronzite spectra of Burns (1970) have been used to get the intensity ratio of the α and β bands at 10800 cm^{-1}.

tion of spin-orbit splitting was carried out in the weak-field coupling scheme. The quantization direction was chosen to be along the Y direction, as mentioned earlier. The basis states were taken to be $|\ ^5D, J\ J_z >$ where $J = 0, 1, 2, 3, 4$. Apart from the cubic term, the crystal field potential in this coordinate system is of the form $B_2^{0'}\ C_2^0 + B_2^{2'}\ [C_2^2 - C_2^{-2}]$. We therefore have to diagonalize a 25×25 hermitian matrix. The procedure for calculating spin-orbit and crystal field matrix elements has been discussed in many books, including Wybourne (1965, pp. 38, 164). The matrix was first converted to a real one and diagonalized. Griffith (1961) quotes a spin-orbit parameter of 410 cm^{-1} for the Fe^{2+} ion and the value for the ferrous ion in a solid is likely to be somewhat reduced. Results for a spin-orbit parameter value of 400 cm^{-1} are shown in Table 5. It is to be noted that spin-orbit splitting is very small due to the quenching effect of the lower symmetry crystal field. The splittings of the 10800, 5400 and 3100 cm^{-1} bands are small compared to the observed band widths and can therefore be safely neglected. Physically, transitions will occur most strongly between states with the same spin composition, and so there is relatively little effect when some of the lowest states are partially depopulated at low temperatures.

It is interesting to note the existence of the first excited level at 1.5 cm^{-1}. The existence of a low-lying level has been confirmed by a preliminary paramagnetic spectrum obtained by J. Le Marshall, A. Tirkel, and G. J. Troup of the Department of Physics, Monash University. Resonance was obtained at a frequency of 70 GHz and a magnetic field of 5kG with the enstatite crystal at 4.2K. The magnetic field direction was normal to the β axis and made angles of 57° and 33° respectively with the α and γ axes. More detailed resonance and far infrared measurements are needed to refine the analysis of the effects of spin-orbit interaction.

The visible spectrum of enstatite (Fig. 3) consists of weak spin-forbidden transitions to the triplet states. Since most of the bands are broad and mutually overlapping, it is difficult to identify the position of individual bands. However, the broad band at about 15500 cm^{-1} can be assigned to transitions to the lowest $^3T_1$ and $^3T_2$ levels and the narrow band at 19780 cm^{-1} is probably due to the transition to the lowest ^3E level. Alternatively Burns (1970) has proposed that bands around 15000 cm^{-1} are due to $Fe^{2+} - Fe^{3+}$ charge transfer.

TABLE 5. Spin-Orbit Splitting of ^5D Levels

O_h	Level Assignment C_{2v} Without Spin-orbit	Level Assignment C_{2v} With Spin-orbit	Level Positions (cm^{-1}) Without Spin-orbit	Level Positions (cm^{-1}) With Spin-orbit
		A_1		10864
		A_2		10862
	$^5A_1$	B_2	10844	10855
		B_1		10845
		A_1		10844
^5E		B_1		5534
		B_2		5533
	$^5B_1$	A_1	5487	5494
		A_2		5478
		B_1		5466
		A_2		5100
		B_2		5090
	$^5A_2$	A_1	5041	5053
		B_1		5008
		A_2		5003
		A_1		3131
		B_2		3131
$^5T_2$	$^5B_2$	A_2	3108	3113
		B_1		3113
		B_2		3106
		A_1		19
		A_2		18
	$^5A_1$	B_2	0	9
		B_1		1.5
		A_1		0

Band Intensities

The most distinctive feature of the spectrum is the very intense α band at 10800 cm^{-1}. In O_h, D_{4h}, or D_{2h} symmetry the transitions $^5T_g \rightarrow {}^5E_g$ are parity forbidden, and could be observed only due to vibronic coupling of odd-parity vibrational modes. In C_{2v} symmetry the transitions are allowed, and the wave functions will be mixed with odd-parity states. In the crystal the lowest odd-parity states will be charge-transfer states and it is reasonable to suppose that the lowest state will have the symmetry of the nearest neighbor ions and belong to the A_1 representation of C_{2v}. This assumption could in principle be checked by a molecular orbital calculation, but in practice this would be a formidable procedure. At 27000 cm^{-1} the α band is strongest, as expected on this basis, and the lowest charge transfer band is tentatively located around 50000 cm^{-1}. The other charge-transfer bands are located on Figure 5 at 90000 cm^{-1}, but the exact positions of the charge-transfer bands are not critical. Consequently, the explanation for the strong α band at 10800 cm^{-1} is

now clear. The A_1 states have heavier odd-parity mixing than the other states due to the relatively low lying A_1 charge-transfer band.

The intensity calculation depends on the odd-parity crystal field. The first order field can be neglected as the ion has to be on a site of minimum energy. Hence the most important contributions are due to third order terms. The only third order terms with A_1 symmetry in C_{2v} arise from the following terms:

T_{1uz} which transforms as

$$\frac{1}{\sqrt{2}}\left[\frac{5(x^3+y^3)}{r^3}-\frac{3(x+y)}{r}\right]$$

and T_{2uX} which transforms as

$$\frac{1}{\sqrt{2}}\left[\frac{y(z^2-x^2)}{r^3}-\frac{x(y^2-z^2)}{r^3}\right].$$

Also the calculations depend on the nature of the odd charge-transfer states which mix into the even E_g and T_{2g} states. The only states which can mix into A_1 states are T_{1uZ} and T_{2uX} states. Fortunately it is not necessary to specify the detailed nature of the charge transfer states in a simplified treatment, as it will be assumed that only the lowest odd-parity A_1 state is significant. The radial overlap integrals between this state and the lower states will be nearly equal and are assumed to be exactly equal. Using these assumptions the relative intensities simply depend on coupling coefficients and the energies of the levels concerned. The four cases depending on the nature of the crystal field and charge transfer state will be considered. The real situation is expected to be a combination of these cases. The coupling coefficients were obtained by rotation of axes of the coupling coefficients in Griffith (1961) (pp. 396–398) using the new coordinate axes $X = [100]$, $Y = [001]$ and $Z = [110]$. Lohr (1970) has published similar coupling coefficients. The calculation will be most easily understood by considering one case in detail.

Intensity Calculations

Case A: Crystal field T_{1uZ}, charge transfer state T_{2uX}

The admixture of the odd-parity state into the even-parity A_1 states is given by a coupling coefficient expressing the effect of the crystal field operation, divided by the energy difference of the states. The transition probability is given by another coupling coefficient between the odd- and even-parity states due to the electric dipole operator. The Einstein B coefficient is proportional to the sum of the squares of the products of these terms for the mixing into the T_{2g} and E_g states.

TABLE 6. Intensity Ratios

Crystal field symmetry	T_{1uZ}	T_{1uZ}	T_{2uX}	T_{2uX}
Charge transfer state	T_{1uZ}	T_{2uX}	T_{1uZ}	T_{2uX}
$\frac{\alpha_Z}{\alpha_X}\cdot\frac{E_3}{E_2}$	$\frac{2}{3}$	6	$\frac{4}{3}$	4
$\frac{\alpha_Y}{\alpha_X}\cdot\frac{E_5}{E_2}$	1	3	1	3

In this case

$$B \propto \frac{[<T_{2gY}\,|T_{1uZ}|\,T_{2uX}><T_{2uX}\,|Z|\,E\theta>]^2}{(E_1)^2} + \frac{[<T_{2gY}\,|Z|\,T_{2uX}><T_{2uX}\,|T_{1uZ}|\,E\theta>]^2}{(E_1-E_2)^2}$$

where E_1 is the energy of the odd-parity A_1 state and E_2 is the energy of the ${}^5E_g$, A_1 state.

The absorption coefficient α is proportional to the oscillator strength f, which is proportional to BE where E is the energy of the transition being considered.

Substitution of the coupling coefficients gives

$$\alpha_Z \propto \left[\frac{1}{4E_1^2}+\frac{1}{4(E_1-E_2)^2}\right]E_2$$

also

$$\alpha_X \propto \frac{E_3}{12E_1^2} \quad \text{and} \quad \frac{\alpha_Z}{\alpha_X}\cdot\frac{E_3}{E_2}=6 \quad \text{when} \quad E_1 \gg E_2,$$

where E_3 is the energy of the ${}^5E_g$, B_1 state. Similarly

$$\alpha_Y \propto \frac{E_5}{4E_1^2} \quad \text{and} \quad \frac{\alpha_Y}{\alpha_X}\cdot\frac{E_5}{E_2}=3,$$

where E_5 is the energy of the ${}^5T_{2g}$, B_2 state.

Intensity ratios for all four cases are listed in Table 6 for $E_1 \gg E_2$. From the spectrum for orthopyroxene in Burns (1970), $\alpha_Z/\alpha_X \cdot E_3/E_2$ is estimated to be about 2.4. Therefore the conclusion is that the charge transfer state must contain a substantial component of T_{2uX} symmetry. Since $E_1 \approx 5E_2$, the approximation $E_1 \gg E_2$ is quite good, but if it is not made $\alpha_Z/\alpha_X \cdot E_3/E_2$ is increased by about 12 percent.

Conclusions

The main features of the polarized spectra of enstatite have been accounted for on a theoretical model using an idealized C_{2v} symmetry. The band intensities are explained in terms of a mixing of states involving the lowest charge transfer state, which is assumed to have A_1 symmetry. Charge transfer states have been discussed previously (Turner, 1967; White, 1967) in connection with the optical spectrum, but the discussion has been qualitative. The ideas developed in the present paper have wide potential application, and will be applied to olivine in Part II (Runciman, Sengupta, and Gourley, 1973) whose acknowledgments apply equally to this paper.

References

Bancroft, G. M., and R. G. Burns (1967) Interpretation of the electronic spectra of iron in pyroxenes. *Amer. Mineral.* **52,** 1278–1287.

Burns, R. G. (1970) *Mineralogical Applications of Crystal Field Theory*. Cambridge University Press.

Cotton, F. A. (1963) *Chemical Applications of Group Theory*. Interscience Publishers, New York.

Ghose, S. (1965) Mg^{2+} — Fe^{2+} order in an orthopyroxene, $Mg_{0.93}Fe_{1.07}Si_2O_6$. *Z. Kristallogr.* **122,** 81–99.

Griffith, J. S. (1961) *The Theory of Transition-metal Ions*. Cambridge University Press.

Lohr, L. L. (1970) Coupling coefficients for the octahedral group with orthorhombic components. *Theoret. Chim. Acta,* **16,** 373–376.

Runciman, W. A., D. Sengupta, and J. T. Gourley (1973) The polarized spectra of iron in silicates. II. Olivine. *Amer. Mineral.* **58,** 451–456.

Turner, W. H. (1967) Optical absorption spectra of iron in the rock forming silicates: a discussion. *Amer. Mineral.* **52,** 553–555.

White, W. B. (1967) Optical absorption spectra of iron in the rock-forming silicates: Reply. *Amer. Mineral.* **52,** 555–558.

———, and K. L. Keester (1966) Optical absorption spectra of iron in the rock-forming silicates. *Amer. Mineral.* **51,** 774–791.

———, and ——— (1967) Selection rules and assignments for the spectra of ferrous iron in pyroxenes. *Amer. Mineral.* **52,** 1508–1514.

Wilson, E. B., J. C. Decius, and P. C. Cross (1955) *Molecular Vibrations*. McGraw-Hill, New York.

Wybourne, B. G. (1965) *Spectroscopic Properties of Rare Earths*. Interscience Publishers, New York.

Manuscript received, July 17, 1972; accepted for publication, December 27, 1972.